Available online at www.sciencedirect.com
SCIENCE DIRECT®
Journal of Molecular Spectroscopy 233 (2005) 278–283
Journal of MOLECULAR SPECTROSCOPY
www.elsevier.com/locate/jms

Rotational analysis of the $\tilde{C}^2A_1$–$\tilde{X}^2A_1$ transition of $SrNH_2$

P.M. Sheridan [a], M.J. Dick [b], J.-G. Wang [a], P.F. Bernath [a,b,*]

[a] Department of Chemistry, University of Waterloo, Waterloo, Ont., Canada N2L 3G1
[b] Department of Physics, University of Waterloo, Waterloo, Ont., Canada N2L 3G1

Received 26 May 2005; in revised form 11 July 2005

Abstract

The $\tilde{C}^2A_1$–$\tilde{X}^2A_1$ electronic transition of $SrNH_2$ has been recorded at high resolution using laser-ablation/molecular jet techniques. Transitions arising from the $K_a'' = 0$ and $K_a'' = 1$ levels have been observed. The data have been analyzed using the *S*-reduced asymmetric top Hamiltonian to determine rotational and fine structure parameters. The spin–rotation constants of the $\tilde{C}^2A_1$ state were calculated using the pure precession model. These values were found to be in relatively good agreement with the experimentally determined parameters, however slight differences suggest that the unpaired electron in the $\tilde{C}^2A_1$ state is not entirely of *p* orbital character. A molecular structure was also determined for the $\tilde{C}^2A_1$ state of $SrNH_2$. The strontium–nitrogen bond was found to decrease by 0.011 Å while the H–N–H bond angle was found to increase by 2.5° between the $\tilde{X}^2A_1$ and $\tilde{C}^2A_1$ states. A small positive inertial defect was calculated for the $\tilde{C}^2A_1$ state, indicating that the molecule is planar.

Keywords: $SrNH_2$; Strontium-containing molecules; Monoamides; Laser spectroscopy; Alkaline-earth metal bond

1. Introduction

Unlike their diatomic counterparts, polyatomic molecules containing alkali and alkaline-earth metal atoms have been the subject of far fewer gas phase spectroscopic studies [1]. In particular this is the case for non-linear polyatomic ligands, which have remained largely uninvestigated at high resolution, most likely the result of the congested nature of their spectra due to their decreased molecular symmetry. One class of these species is the metal monoamides (MNH_2), which have been the focus of several recent spectroscopic investigations that will be summarized below.

For the alkali metals, experimental studies are limited to the amides of lithium and sodium. The pure rotational spectra of both molecules and their deuterium isotopologues have been measured using millimeter-wave spectroscopy in their $\tilde{X}^1A_1$ ground states [2,3]. In these investigations each species was found to exhibit a planar geometry with no evidence of fluxional behavior. Because of interest in these molecules as reagents in organic chemistry, many structure calculations exist for these species (see [2]), however, information about their excited electronic states is non-existent.

The alkaline-earth amides have been the subject of more extensive spectroscopic investigations. Harris and co-workers [4,5], using laser spectroscopic techniques, first reported low resolution spectra of calcium, strontium, and barium amides. The Bernath group [6], in their investigations of various alkaline-earth containing polyatomic species, recorded low resolution spectra of several monoalkylamide derivatives of calcium and strontium. The first laser-ablation study of the $\tilde{A}^2B_2$–$\tilde{X}^2A_1$ and $\tilde{B}^2B_1$–$\tilde{X}^2A_1$ transitions of $CaNH_2$ was performed by Whitham et al. [7,8] at medium resolution. This work was superseded by high resolution analyses of the $\tilde{A}^2B_2$–$\tilde{X}^2A_1$, $\tilde{B}^2B_1$–$\tilde{X}^2A_1$, and $\tilde{C}^2A_1$–$\tilde{X}^2A_1$ electronic transitions of $CaNH_2$ by laser spectroscopy [9–11]. In

* Corresponding author. Fax: +1 519 746 0435.
E-mail address: bernath@uwaterloo.ca (P.F. Bernath).

0022-2852/$ - see front matter © 2005 Published by Elsevier Inc.
doi:10.1016/j.jms.2005.07.011

addition, the dipole moment in the ground state of $CaNH_2$ was measured using optical Stark spectroscopy [9]. For strontium amide, the $\tilde{A}^2B_2$–$\tilde{X}^2A_1$ and $\tilde{B}^2B_1$–$\tilde{X}^2A_1$ transitions have been rotationally analyzed using high resolution laser spectroscopy, while the $\tilde{C}^2A_1$–$\tilde{X}^2A_1$ transition has been observed only at low resolution [12]. Finally, the pure rotational spectra of magnesium, calcium, and strontium amides have been recorded along with their deuterium isotopologues [13–16]. Again, each species was found to be planar and an r_0 structure was determined in the ground state. Theoretical investigations of these species are limited to electron propagator calculations of excited state energies of $CaNH_2$ by Ortiz [17] and ground state geometry and vibrational frequency calculations of both calcium and strontium amide [18]. No additional metal amide species have been observed experimentally.

In this paper, we present a rotational analysis of our high resolution spectrum of the $\tilde{C}^2A_1$–$\tilde{X}^2A_1$ transition of strontium amide. This work completes the high resolution observation of the four lowest electronic states of $SrNH_2$. In addition, $SrNH_2$ is now the second non-linear alkaline-earth containing molecule ($CaNH_2$ is the other) for which these four states have been investigated. In this analysis, rotational and fine structure parameters have been determined for the $\tilde{C}^2A_1$ state. Here, we present these results as well as a discussion of the spin–rotation constants in terms of the pure precession model and the molecular structure of $SrNH_2$.

2. Experimental

The $\tilde{C}^2A_1$–$\tilde{X}^2A_1$ transition of $SrNH_2$ was observed using the laser-ablation source of the Bernath group [19] at the University of Waterloo, which has been described in detail previously. Briefly, the third harmonic (355 nm) of a pulsed (10 Hz) Nd/YAG laser (10 mJ/pulse) was used to vaporize a strontium target rod. A free jet expansion was formed using a 15% gas mixture of NH_3 in Ar at a backing pressure of 100 psi, resulting in a rotational temperature of only 4–6 K. The probe laser then interrogated this expansion ~15 cm downstream. Band pass filters (±20 nm) were used to attenuate most of the plasma radiation from the ablation source. The signal from the PMT was sent through a preamplifier (100× current amplifier) and processed using a boxcar integrator.

High resolution spectra were obtained using a Coherent Autoscan 699-29 ring dye laser system. This laser has a line width of about 10 MHz. The spectra were calibrated using I_2 lines [20], which were recorded at the same time as the experimental data. A typical spectrum was taken in 5 cm^{-1} segments at a scan speed of 60 s per cm^{-1} with a data sampling rate of about 10 MHz. Typical experimental line widths of 350 MHz were observed as a result of residual Doppler broadening of the molecular jet as it passed through the detection region.

3. Results and analysis

Using the approximate band center from the previous low resolution work [12], a high resolution spectrum of the $\tilde{C}^2A_1$–$\tilde{X}^2A_1$ transition of $SrNH_2$ was measured. The $\tilde{C}^2A_1$ state correlates to a $^2\Sigma^+$ state in the linear limit, such as the $B^2\Sigma^+$ state of CaF [11]. Therefore, the appearance of this electronic transition should be similar to a Hund's case (b) $^2\Sigma$–case (b) $^2\Sigma$ transition, with a line spacing of ~2B. In Fig. 1, a high resolution spectrum of the $\tilde{C}^2A_1$–$\tilde{X}^2A_1$ transition of $SrNH_2$ is shown. The condensed nature of this spectrum is consistent with a parallel type transition.

Strontium amide is a planar, near prolate asymmetric top molecule with C_{2v} symmetry [12,16]. The dipole moment lies along the a molecular axis (strontium–nitrogen bond), which gives rise to the selection rule $\Delta K_a = 0$. Rotation about the a axis exchanges the two protons giving rise to two nuclear spin states, *ortho* (K_a odd) and *para* (K_a even). As a result, the molecules can only be cooled into either the $K_a'' = 0$ levels (*para*) or the $K_a'' = 1$ levels (*ortho*); therefore, transitions originating from both levels are expected to be present in the spectrum. This is in contrast to SrSH for which we find transitions from the $K_a'' = 1$ levels to be weak. Under our jet expansion conditions the $K_a'' = 1$ levels of $SrNH_2$ are metastable because of nuclear spin statistics.

Nuclear spin statistics affect the line intensities of $SrNH_2$, enhancing the strength of the odd K_a levels com-

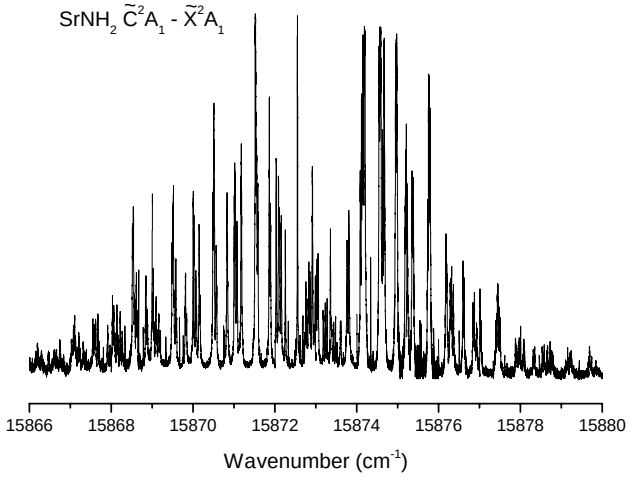

Fig. 1. High resolution spectrum of the $\tilde{C}^2A_1$–$\tilde{X}^2A_1$ electronic transition of $SrNH_2$ over the range 15866–15880 cm^{-1}. The spectrum has the appearance of a Hund's case (b) $^2\Sigma$–case (b) $^2\Sigma$ transition. Transitions arising from both the $K_a = 0$ and $K_a = 1$ sub-bands are present, resulting in a congested appearance due to their similar band origins.

pared to the even K_a levels by ~3:1. As a result, the spectrum appears quite complicated due to sub-bands arising from the $K_a'' = 0$ and $K_a'' = 1$ energy levels being present, both having nearly the same origin. Sub-bands with $K_a > 1$ are not present due to the cold rotational temperature of the molecules.

The energy level diagram showing the allowed transitions of the $K_a = 0$ sub-band of the $\tilde{C}^2A_1$–$\tilde{X}^2A_1$ transition of $SrNH_2$ is presented as Fig. 2. Each rotational level is split into two spin–rotation components, labeled as F_1 ($J = N + 1/2$) and F_2 ($J = N - 1/2$). The branch structure resembles that of a Hund's case (b) $^2\Sigma$–case (b) $^2\Sigma$ transition. Each energy level is labeled by the asymmetric top quantum numbers N, K_a, K_c, and J. The selection rule $\Delta J = \Delta N = \pm 1$ gives rise to two P and R branches; also possible are two satellite Q branches where $\Delta N = \pm 1$ and $\Delta J = 0$. Transitions belonging to each of these six branches were observed for $SrNH_2$.

An energy level diagram of the $K_a = 1$ sub-band of $SrNH_2$ is shown in Fig. 3. The F_1 spin component levels are located on the left, while those of the F_2 spin component are found on the right. Again each level is labeled by the quantum numbers N, K_a, K_c, and J. Here, the branch structure for each spin component resembles a

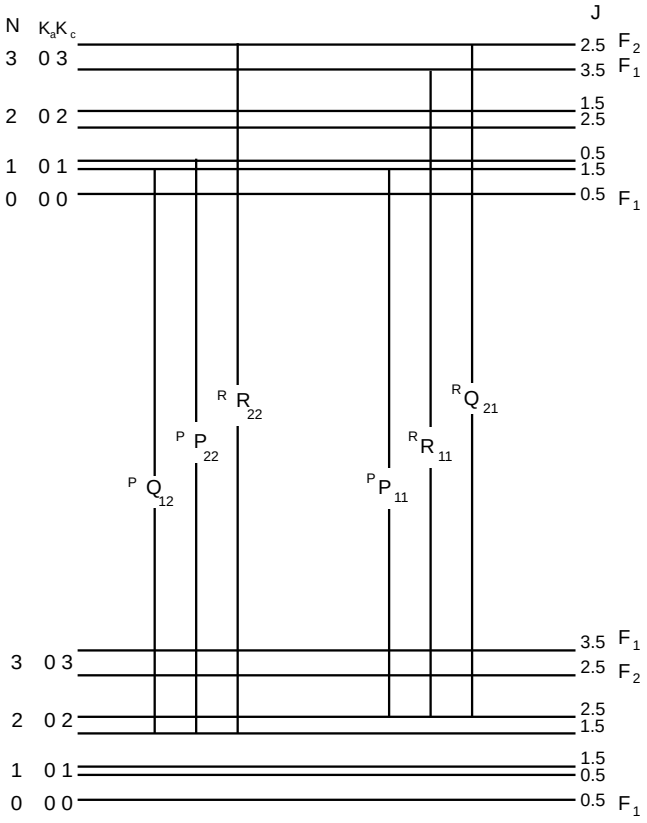

Fig. 2. An energy level diagram of the $K_a = 0$ sub-band of the $\tilde{C}^2A_1$–$\tilde{X}^2A_1$ transition of $SrNH_2$. The energy levels are labeled by the quantum numbers N, K_a, K_c, and J. The six allowed transitions are labeled by the branch notation $^{\Delta N}\Delta J_{F_i', F_j''}$ ($i = 1, 2$; $j = 1, 2$).

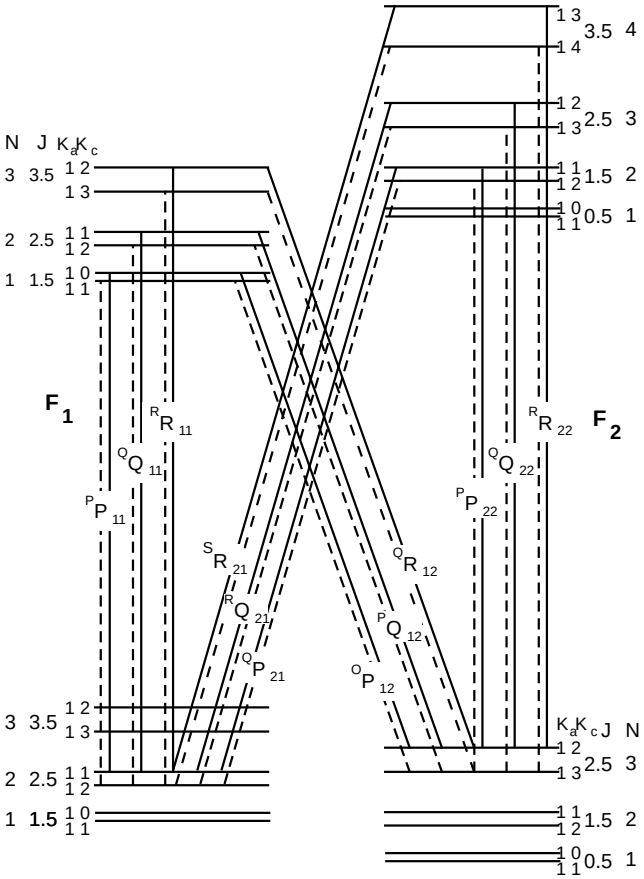

Fig. 3. An energy level diagram showing the allowed transitions of the $K_a = 1$ sub-band of the $\tilde{C}^2A_1$–$\tilde{X}^2A_1$ transition of $SrNH_2$. The levels of the F_1 spin component are located on the left side of the figure and the levels of the F_2 spin component are located on the right. Each level is labeled by the quantum numbers N, K_a, K_c, and J. The 24 possible branches are labeled by the notation $^{\Delta N}\Delta J_{F_i', F_j''}$ ($i = 1, 2$; $j = 1, 2$) with asymmetry components indicated by their γ values (see text) solid lines: $\gamma = 0$; dashed lines: $\gamma = 1$.

Hund's case (b) $^2\Pi$–case (b) $^2\Pi$ transition. The selection rule $\Delta J = \Delta N = 0, \pm 1$ gives rise to three branches (^PP, ^QQ, and ^RR) within each F_1 and F_2 spin component. A further splitting can occur within each branch as a result of asymmetry doubling. Each asymmetry component is labeled by the quantity $\gamma = K_a + K_c - N$, which gives rise to values of $\gamma = 0$ and 1 [11]. In Fig. 3, $\gamma = 0$ transitions are shown as solid lines, while $\gamma = 1$ transitions are shown as dashed lines. In addition, six satellite branches ($\Delta J \neq \Delta N$; $\Delta J = 0, \pm 1$; $\Delta N = 0, \pm 1, \pm 2$) are possible, each of which is also subject to asymmetry splitting. Transitions in all of the 24 possible branches of the $K_a = 1$ sub-band were observed for $SrNH_2$.

Despite the highly congested nature of the $\tilde{C}^2A_1$–$\tilde{X}^2A_1$ spectrum of $SrNH_2$, individual P and R branches could be identified with minimal difficulty. Due to the large spin–rotation interaction in the $\tilde{C}^2A_1$ state, each branch could be identified as arising from either the F_1 or F_2 levels by examining the relative spacing of the lines. How-

ever, matching the corresponding P and R branches and assigning J values were more arduous tasks. Ground state combination differences, available from the millimeter-wave work [16], were used to make assignments. Initially, the corresponding P and R ($K_a = 0$) branches were matched in this manner and then added to the fitting program. Satellite branches were then predicted to further confirm the correctness of the fit. This procedure was then repeated with the remaining branches ($K_a = 1$), which proved more difficult to identify due to the asymmetry splitting. Branch assignments were also aided by using the $\tilde{C}^2A_1$–$\tilde{X}^2A_1$ transition of $CaNH_2$ as a guide [11].

In Fig. 4, a short section of the high resolution spectrum of the $\tilde{C}^2A_1$–$\tilde{X}^2A_1$ transition of $SrNH_2$ is shown with branch assignments. Lines arising from the $K_a = 0$ sub-band are labeled on top, while those belonging to the $K_a = 1$ sub-band are identified below. The quantum number J appears above each line. In the $K_a = 0$ sub-band, the line spacing of the $^PP_{11}$ branch is larger than in the $^PP_{22}$ branch, a result of the larger spin–rotation interaction in the $\tilde{C}^2A_1$ state as compared to the $\tilde{X}^2A_1$ state. Also, the $^PP_{11}$ and $^PQ_{12}$ branches follow each other closely, slowly separating with increasing J. For the $K_a = 1$ sub-band, the γ value of the asymmetry components of the branches shown are indicated by the length of the vertical line below the J assignment (shorter line, $\gamma = 0$; longer line, $\gamma = 1$). Again, the line spacing of the $^PP_{11}$ branch is greater than in the $^PP_{22}$ branch in the $K_a = 1$ sub-band. Of the branches shown, the asymmetry components of the $^PQ_{12}$ branch exhibit the largest splitting. Because of the high signal-to-noise ratio present in the spectrum, two features at $\sim$15870.75 cm^{-1} belonging to the weaker $^OP_{12}$ branch, shown on the bottom, were observed.

The data measured for the $\tilde{C}^2A_1$–$\tilde{X}^2A_1$ transition of $SrNH_2$ were fit to the S-reduced asymmetric top Hamiltonian of Watson [21]. The Hamiltonian includes rotational and spin–rotation parameters as well as the higher order centrifugal distortion terms used in the millimeter-wave analysis [16]. A least squares fit of the data was accomplished using the program SPFIT of Pickett [22]. For $SrNH_2$, 240 lines arising from the $K_a = 0$ and $K_a = 1$ sub-bands ($J \leqslant 19.5$), as well as the pure rotational data [16], were included in the final fit. The measured lines are available as supplemental material from the journal. The pure rotational data were included so that proper errors could be determined for the $\tilde{C}^2A_1$ state. Estimated errors of the pure rotational and optical data used as weighting factors in the program were 100 kHz and 0.005 cm^{-1}, respectively. Spectroscopic constants for both the $\tilde{C}^2A_1$ and $\tilde{X}^2A_1$ states were allowed to vary and are listed in Table 1. Also included in Table 1, for comparison, are the parameters for the

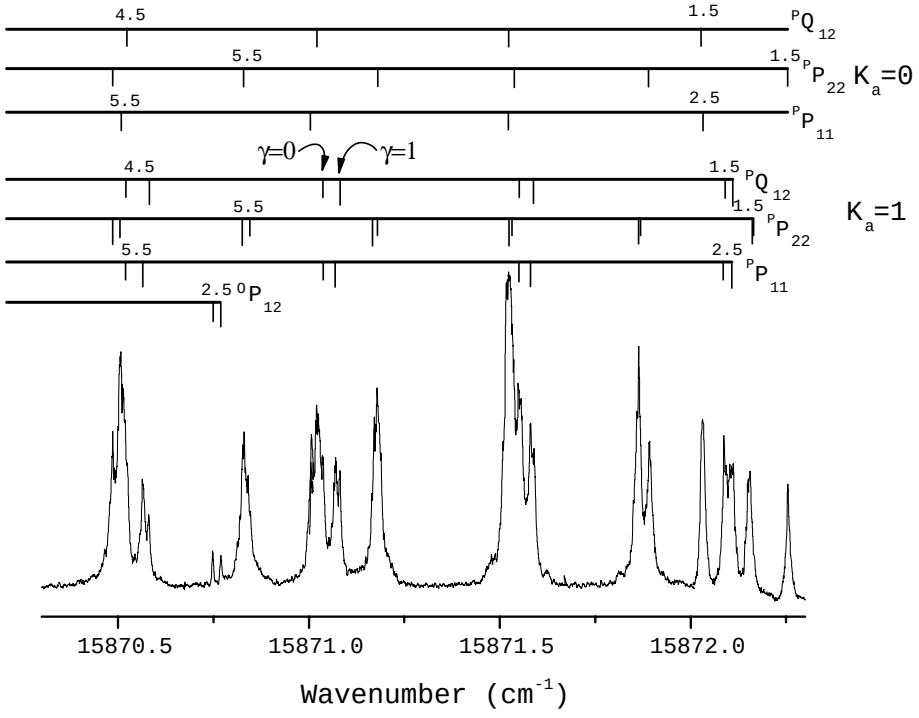

Fig. 4. A sub-section of the high resolution spectrum of the $\tilde{C}^2A_1$–$\tilde{X}^2A_1$ transition of $SrNH_2$. The branches for the $K_a = 0$ and $K_a = 1$ sub-bands are identified on the top and bottom, respectively. For both the $K_a = 0$ and $K_a = 1$ sub-bands, the line spacing is greater in the $^PP_{11}$ branch than in the $^PP_{22}$ branch due to the large spin–rotation interaction in the $\tilde{C}^2A_1$ state. The γ value (see text) of the asymmetry components is indicated by the length of the vertical line below the J assignment (shorter line, $\gamma = 0$; longer line, $\gamma = 1$). Because of the high signal-to-noise ratio present in the spectrum, the two features at $\sim$15870.75 cm^{-1} could be identified as belonging to the weaker $^OP_{12}$ branch.

Table 1
Spectroscopic parameters (in cm^{-1}) for the $\tilde{C}^2A_1$ and $\tilde{X}^2A_1$ states of $SrNH_2$

Parameter	$\tilde{X}^2A_1$ [a]	$\tilde{X}^2A_1$ [b]	$\tilde{C}^2A_1$ [b]
T	0.0	0.0	15872.99759(75)
ε_{aa}	0.005350(77)	0.005339(78)	0.0869(32)
ε_{bb}	0.0019927(29)	0.0019927(19)	−0.16001(24)
ε_{cc}	0.0029906(27)	0.0029906(18)	−0.13388(24)
A_{NK}^{S}	$-1.83(40)\times10^{-10}$	$-1.85(30)\times10^{-10}$	
A	13.1538(47)	13.1542(21)	13.1744(23)
B	0.22649990(9)	0.226499903(58)	0.229281(16)
C	0.22213754(9)	0.222137549(55)	0.224498(16)
D_N	$2.02652(25)\times10^{-7}$	$2.02655(10)\times10^{-7}$	$4.72(47)\times10^{-7}$
D_{NK}	$4.5348(47)\times10^{-5}$	$4.5373(11)\times10^{-5}$	
d_1	$-5.135(15)\times10^{-9}$	$-5.135(10)\times10^{-9}$	
d_2	$-1.649(28)\times10^{-9}$	$-1.647(18)\times10^{-9}$	
h_2	$4.4(1.3)\times10^{-14}$	$4.33(86)\times10^{-14}$	
h_3	$9.8(2.1)\times10^{-15}$	$9.8(1.4)\times10^{-15}$	
H_{NK}	$7.71(43)\times10^{-10}$	$7.635(37)\times10^{-10}$	
H_{KN}	$-2.068(60)\times10^{-7}$	$-2.0081(88)\times10^{-7}$	
L_{NNK}	$-3.0(2.0)\times10^{-14}$		
L_{NK}	$5.3(4.3)\times10^{-11}$		
L_{KKN}	$-4.61(15)\times10^{-9}$	$-4.653(29)\times10^{-9}$	
P_{NNK}	$-3.34(73)\times10^{-15}$	$-1.97(13)\times10^{-15}$	
P_{NKK}	$7.54(97)\times10^{-13}$	$7.74(19)\times10^{-13}$	
P_{NK}	$1.10(50)\times10^{-17}$		

[a] Millimeter-wave work [16].
[b] This work. Values in parenthesis are 1σ standard deviations, in units of the last significant digits.

ground state as determined from the pure rotational data (estimated error 50 kHz) [16]. As can be seen there is relatively good agreement between the current parameters and those of the previous work. Inconsistencies that occur with the higher order constants are the result of the larger experimental uncertainties we chose for the millimeter-wave data in our fit. For the $\tilde{C}^2A_1$ state, in addition to the rotational and spin–rotation constants, only one centrifugal distortion constant, D_N, could be determined because of the low J values observed in this work.

4. Discussion

It has been shown previously that the spin–rotation interaction is dominated by second order effects [11]. Using the pure precession model and the unique perturber approximation, the three spin–rotation constants for a molecule with orthorhombic symmetry, ε_{aa}, ε_{bb}, and ε_{cc}, can be calculated. The pure precession relationships for these parameters have been derived in the analysis of the $\tilde{C}^2A_1$–$\tilde{X}^2A_1$ transition of $CaNH_2$ [11]. For the $\tilde{C}^2A_1$ state of $SrNH_2$, the relevant equations are:

$$\varepsilon_{bb} = \frac{-2l(l+1)BA^{so}}{\Delta E_{\tilde{C}-\tilde{B}}} \quad (1)$$

and

$$\varepsilon_{cc} = \frac{-2l(l+1)CA^{so}}{\Delta E_{\tilde{C}-\tilde{A}}}. \quad (2)$$

If we assume that the unpaired electron in the $\tilde{C}^2A_1$ state is in a pure p orbital (p_z), then a value of $l = 1$ can be used. If A^{so} from SrOH (264 cm^{-1}) is employed [23], then ε_{bb} and ε_{cc} are calculated to be −0.205 and −0.144 cm^{-1}, respectively. These values are in reasonably good agreement with those determined experimentally: $\varepsilon_{bb} = -0.16001(24)$ cm^{-1} and $\varepsilon_{cc} = -0.13388(24)$ cm^{-1}. Differences between the experimental and calculated parameters most likely arise from the assumption that the unpaired electron in the $\tilde{C}^2A_1$ state can be entirely described as being in a p orbital. This implies that the unpaired electron in the $\tilde{C}^2A_1$ state must be a mixture of some other orbital character (most likely d). The presence of non-p orbital character in the unpaired electron is further suggested by the small positive value of ε_{aa} (0.0869 cm^{-1}), which is calculated to be zero by the pure precession model.

The $\tilde{A}^2B_2$ and $\tilde{B}^2B_1$ states of both $CaNH_2$ and $SrNH_2$ have been shown to interact strongly via a Coriolis-type interaction [9,10,12]. Therefore, the A rotational constant is affected, resulting in a value that implies a greater structural change than expected. As a result, second order corrections to the A rotational constant had to be considered to obtain a correct molecular structure in the $\tilde{A}^2B_2$ and $\tilde{B}^2B_1$ states. While second order contributions to the B and C rotational constants are also possible, they were found to be less than the experimental error for the $\tilde{A}^2B_2$ and $\tilde{B}^2B_1$ states of $CaNH_2$ and $SrNH_2$. In the $\tilde{C}^2A_1$ state of $CaNH_2$, again the second order contributions to the three rotational constants were found to be minimal and therefore neglected [11];

Table 2
Structural parameters for the low-lying electronic states of $SrNH_2$

State	r_{Sr-N} (Å)	r_{N-H} (Å)[a]	θ_{H-N-H} (°)
$\tilde{X}^2A_1$[b]	2.256	1.021	105.5
$\tilde{A}^2B_2$[c]	2.235	1.021	105.3
$\tilde{B}^2B_1$[c]	2.238	1.021	105.2
$\tilde{C}^2A_1$	2.245	1.021	108.0

[a] Held fixed to millimeter-wave value [16].
[b] From [16].
[c] Using rotational constants of [12].

the same situation was found in this work for the $\tilde{C}^2A_1$ state of $SrNH_2$.

Molecular structures have been previously reported for the $\tilde{X}^2A_1$, $\tilde{A}^2B_2$, and $\tilde{B}^2B_1$ states of $SrNH_2$ [12]. However, in each case only one isotopologue was observed, therefore the N–H bond length was fixed to that of NH_2^- (1.041 Å). In the subsequent millimeter-wave investigation [16], rotational spectra of both $SrNH_2$ and $SrND_2$ were analyzed and the rotational constants were used to determine an r_0 structure for the ground state. In this work, the r_{N-H} value was found to be 1.021 Å. If r_{N-H} is fixed to the millimeter-wave value, more accurate Sr–N bond lengths and H–N–H bond angles can be calculated for the $\tilde{A}^2B_2$, $\tilde{B}^2B_1$, and $\tilde{C}^2A_1$ states of $SrNH_2$. Using a least squares fit to the moment of inertia equations [24], these new structural parameters were determined and are listed in Table 2. For $SrNH_2$, the Sr–N bond length is slightly shorter in the $\tilde{A}^2B_2$, $\tilde{B}^2B_1$, and $\tilde{C}^2A_1$ states compared to the $\tilde{X}^2A_1$ state. This behavior has been observed in the excited states of linear strontium containing molecules such as SrOH [23,25]. This shortening implies that the unpaired electron becomes more polarized away from the metal–nitrogen bond in these excited states. The H–N–H bond angle changes little between the $\tilde{X}^2A_1$, $\tilde{A}^2B_2$, and $\tilde{B}^2B_1$ states; however a small increase of 2.5° is found in the $\tilde{C}^2A_1$ state. In the $\tilde{C}^2A_1$ state, the unpaired electron is expected to be polarized away from the molecule, which in turn may allow for the H–N–H bond angle to open. The inertial defect in the $\tilde{C}^2A_1$ state is 0.287 amu Å^2 consistent with a planar structure.

Acknowledgment

Financial support for this work was provided by the Natural Sciences and Engineering Research Council (NSERC) of Canada.

Appendix A. Supplementary data

Supplementary data for this article are available on ScienceDirect (www.sciencedirect.com) and as part of the Ohio State University Molecular Spectroscopy Archives (http://msa.lib.ohio-state.edu/jmsa_hp.htm).

References

[1] P.F. Bernath, Adv. Photochem. 23 (1997) 1–62.
[2] D.B. Grotjahn, P.M. Sheridan, I. Al Jihad, L.M. Ziurys, J. Am. Chem. Soc. 123 (2001) 5489–5494.
[3] J. Xin, M.A. Brewster, L.M. Ziurys, Astrophys. J. 530 (2000) 323–328.
[4] R.F. Wormsbecher, R.E. Penn, D.O. Harris, J. Mol. Spectrosc. 97 (1983) 65–72.
[5] R.F. Wormsbecher, M. Trkula, C. Martner, R.E. Penn, D.O. Harris, J. Mol. Spectrosc. 97 (1983) 29–36.
[6] A.M.R.P. Bopegedra, C.R. Brazier, P.F. Bernath, J. Phys. Chem. 91 (1987) 2779–2781.
[7] C.J. Whitham, B. Soep, J.-P. Visticot, A. Keller, J. Chem. Phys. 93 (1990) 991–1000.
[8] C.J. Whitham, Ch. Jungen, J. Chem. Phys. 93 (1990) 1001–1008.
[9] A.J. Marr, M. Tanimoto, D. Goodridge, T.C. Steimle, J. Chem. Phys. 103 (1995) 4466–4475.
[10] Z. Morbi, C. Zhao, J.W. Hepburn, P.F. Bernath, J. Chem. Phys. 108 (1998) 8891–8898.
[11] Z. Morbi, C. Zhao, P.F. Bernath, J. Chem. Phys. 106 (1997) 4860–4868.
[12] C.R. Brazier, P.F. Bernath, J. Mol. Spectrosc. 201 (2000) 116–123.
[13] P.M. Sheridan, L.M. Ziurys, Can. J. Phys. 79 (2001) 409–421.
[14] P.M. Sheridan, L.M. Ziurys, Astrophys. J. 540 (2000) L61–L64.
[15] M.A. Brewster, L.M. Ziurys, J. Chem. Phys. 113 (2000) 3141–3149.
[16] J.M. Thompsen, P.M. Sheridan, L.M. Ziurys, Chem. Phys. Lett. 330 (2000) 373–382.
[17] J.V. Ortiz, J. Chem. Phys. 92 (1990) 6728–6731.
[18] W.-T. Chan, I.P. Hamilton, Chem. Phys. Lett. 297 (1998) 217–224.
[19] C. Zhao, P.G. Hajigeorgiou, P.F. Bernath, J.W. Hepburn, J. Mol. Spectrosc. 176 (1996) 268–273.
[20] S. Gerstekorn, P. Luc "Atlas du Spectre d'Absorption de la Molecule d'Iode" Laboratoire Aimé-Cotton, CNRS II, 91405, Orsay, France, 1978.
[21] J.K.G. Watson, in: J.R. Durig (Ed.), Vibrational Spectra and Structure, Elsevier, Amsterdam, 1997, p. 1.
[22] H.M. Pickett, J. Mol. Spectrosc. 148 (1991) 371–377.
[23] C.R. Brazier, P.F. Bernath, J. Mol. Spectrosc. 114 (1985) 163–173.
[24] W. Gordy, R.L. Cook, Microwave Molecular Spectra, Wiley, New York, 1984, 503.
[25] J. Nakagawa, R.F. Wormsbecher, D.O. Harris, J. Mol. Spectrosc. 97 (1983) 37–64.